

Output power and threshold gain of apodized DFB fiber laser

A. I. Azmi^{*a,b}, D. Sen^a, and G. D. Peng^a

^aPhotonic and Optical Communications Group, School of Electrical Engineering and Telecommunications, The University of New South Wales, 2052, NSW, Australia

^bTelematics and Optic Communications Engineering Department, Faculty of Electrical Engineering, Universiti Teknologi Malaysia, Skudai 81310 Johor, Malaysia

ABSTRACT

Effects of apodization on distributed feedback fiber laser (DFB FL) output power and threshold gain are theoretically investigated by employing the transfer matrix method. Three distinct types of profile are investigated: the gaussian, flat or nonapodize, and sigmoid profile. The gaussian and sigmoid profiles are the two extreme cases examined; the former has a strong profile around a centrally located phase shift, while the latter is with a weaker profile. Findings indicate that the tradeoff between output power and higher order mode threshold performance are resulting from the interplay between these profile shapes. The comprehensive results presented in this paper should assist the development of high performance DFB FLs.

Keywords: distributed feedback fiber laser; apodization; output power; threshold gain, transfer matrix method

1. INTRODUCTION

Distributed feedback fiber laser (DFB FL) has long been known for its unique characteristics such as narrow spectral linewidth as well as robust single longitudinal mode operation. Due to the low phase noise property manifested by the low spectral linewidth in order of few kHz [1], DFB FL has become the primary choice in sensing application that demands very high sensitivity and resolution. An example of the sensing application is the interferometric based underwater acoustic system [2-4] that are developed for military and industrial usages. Some additional advantages of DFB FL are that it inherently possesses similar characteristics of an optical fiber such as compact in size, ease of multiplexing and demultiplexing and electrically passive that makes it an ideal candidate as a sensing head for underwater environment. Despite being well established in such applications, the design aspect of DFB FL is somehow receiving lack of attention.

This study provides systematic analysis on effects of profile shapes on two main important parameters, namely the output power and threshold gain. The output power parameter depends on the concentration and effectiveness of active dopants that determines gain of the material, which is similar to the conventional fiber amplifier. Due to the complex distributed feedback structure, the output power also relies on the cavity design parameters such as the grating strength and profile shape. These design parameters control the spatial power evolution within the cavity resulting in the effective use of cavity for power conversion. A proper selection of design parameters can only be made by thoroughly examining all possible values of these design parameters. On the other hand, the first higher order mode threshold parameter measures the stability of DFB FL in a single longitudinal mode operation when the gain and grating strength are increased. From DFB FL design perspective, it is advantageous to define threshold in term of grating strength since designer can control this parameter during grating inscription process. Analysis of threshold grating strength for fundamental and higher order mode of flat profile have been presented by [5]. The threshold gain parameter in general, is considered insignificant since the operation of a flat profile DFB FL is normally far below the first higher order mode threshold gain. However, in our perspective, investigation of threshold gain is as important as threshold grating strength considering the two following reasons. Firstly, certain apodization profiles that are designed to improve output power could reduce the threshold margin between fundamental and first higher order mode threshold. Secondly, the emergence of new fiber materials such as phosphate will dramatically improve the level of Yb³⁺ concentration without the degradation of laser efficiency [6-8], and hence will upgrade the net gain close to first higher order mode threshold.

*asrul@student.unsw.edu.au; phone +61 (2) 93856578; fax +61 (2) 93855993

Three distinct types of profile are investigated namely the gaussian, flat and sigmoid to represent three different profile characteristics. The gaussian has a strong profile around the centrally located phase shift while the sigmoid is with weak profile. These three profile shapes are considered in this study because the performance of DFB FL is highly influenced by these characteristics. In the following section, we describe the principles and numerical models implemented for the simulation of apodized DFB FL. Subsequently, we present the results of output power as well as threshold gain and finally we end with the conclusion.

2. NUMERICAL METHOD

Analysis of the output power and threshold gain of apodized DFB FL requires the use of the Transfer Matrix Method (TMM) due to the spatially varying cavity parameters. However, both output power and threshold are determined based on different conditions and hence different techniques are applied. Numerical solution of output power involves the establishment of rate equations to determine the spatial power distribution of pump and signal, as well as spatial gain. The output power is determined by inserting trial values to the TMM until a certain boundary conditions are fulfilled [9]. On the other hand, numerical solution of the threshold gain is based on the above threshold condition analysis. The threshold gain and wavelength are determined when oscillation condition of laser cavity is met, where finite output can be yielded without any input provided [10]. The net gain is considered instead of the spatial gain and therefore the rate equations are excluded from threshold gain analysis. Further details of each numerical method used this work are described in following sections.

2.1 The Transfer Matrix Method

TMM is a piecewise approach that allows spatial parameterized of DFB-FL cavity, thus enabling analysis of spatial varying cavity profile. In this method, DFB FL cavity is divided into a few hundred of sections, with each section carries its respective parameters' properties. The 2X2 transfer matrix components representing each of the DFB FL sections are derived from the Coupled Mode Equations [11] and can be written as:

$$T_{11}^m = \frac{[S^m \cosh S^m L^m - i(\Delta\beta^m + i\gamma^m) \sinh S^m L^m] e^{-i(\beta_0)L^m}}{S^m} \quad (1)$$

$$T_{12}^m = \frac{\kappa^m \sinh S^m L^m e^{-(i\beta_0 L^m + \phi^m)}}{S^m} \quad (2)$$

$$T_{21}^m = \frac{\kappa^m \sinh S^m L^m e^{i(\beta_0 L^m + \phi^m)}}{S^m} \quad (3)$$

$$T_{22}^m = \frac{[S^m \cosh S^m L^m + i(\Delta\beta^m + i\gamma^m) \sinh S^m L^m] e^{i(\beta_0)L^m}}{S^m} \quad (4)$$

where superscript m refers to the m^{th} section of the cavity, i is the complex number defined by $i = \sqrt{-1}$, L^m is the section length, β_0 is the propagation constant of the designed wavelength, $\Delta\beta^m$ is the detuning of the propagation constant from the designed value, γ^m is the gain induced by pump power, κ^m is the AC coupling coefficient, and ϕ^m is the grating phase.

The mathematical definitions of parameters used in solving the TMM are defined as follows:

$$S^m = \sqrt{(\kappa^m)^2 - (i\Delta\beta^m - \gamma^m)^2} \quad (5)$$

$$\lambda_B^m = 2\Lambda^m n_{eff} \quad (6)$$

$$\kappa^m = \pi \Delta n^m / \lambda_B^m \quad (7)$$

$$\Delta\beta^m = 2\pi m_{eff} (1/\lambda_L - 1/\lambda_B^m) \quad (8)$$

$$\varphi^m = \varphi_0 + \sum_{m=1}^{M-1} 2\pi L^m / \Lambda^m \quad (9)$$

where λ_L and λ_B^m are the designed wavelength and actual Bragg wavelength respectively, Λ^m is the grating period, n_{eff} is the effective refractive index, Δn^m is the change refractive index due to photosensitivity effect, φ^m is the grating phase with the initial grating phase of φ_0 and M is the total number of section used in calculation. Another important physical structure is the π -phase shift that sustains single longitudinal operation of DFB FL, is defined by the following matrix form:

$$T_\phi = \begin{bmatrix} \exp(-i\phi/2) & 0 \\ 0 & \exp(i\phi/2) \end{bmatrix} \quad (10)$$

where ϕ is the phase shift value which equal to π .

2.2 The rate equations

The gain of each DFB FL section, γ^n induced by pump power is determined by solving the rate equation of $\text{Er}^{3+}:\text{Yb}^{3+}$ codoped fiber. Er^{3+} ion is normally selected as the doping material in fiber amplifier design since it possesses high emission cross section at 1530nm and 1550nm that is similar to telecommunications band, hence taking advantage of low propagation loss and compatibility to standard telecommunications measurement instruments. Yb^{3+} ion is normally codoped with Er^{3+} as sensitizer due to its high absorption cross section at 980nm and effective energy transfer to Er^{3+} ion. The energy level diagram describing the quantum interactions of signal and pump intensity towards Er^{3+} and Yb^{3+} ions is indicated in Figure 1. Transition of Er^{3+} and Yb^{3+} ions are characterized by 4 and 2 levels atomic systems respectively. The stimulated emission and absorption rate are designated by σ_{pq} , spontaneous decay rate by W_{pq} , and energy transfer rate by C_{pq} . Subscripts p and q represent the initial and final energy levels of a transition. Energy levels involved in the transition are labeled with unique number from 1 to 6 for clarity, e.g. energy level $^4I_{15/2}$ is labeled with 1. The stimulated transition from $^4I_{13/2}$ to $^4I_{15/2}$ is responsible for lasing at 1530nm, and this transition is measured by emission cross section, σ_{21} . Further details of energy level diagram of $\text{Er}^{3+}:\text{Yb}^{3+}$ is described in other literatures [12, 13]. A set of rate equations is developed based on the energy level diagram to express the population changes in time, outlined by equations (11) to (16). Ion population at each energy level is represented by symbol N with the subscript number denoting the corresponding energy level. Complex effects of fiber amplifier such as amplified spontaneous emission (ASE) are omitted in this model for simplicity. All parameters values are carefully chosen to closely simulate the actual process of quantum optics in the fiber laser. These values are determined by either referring to the results obtained from other literature or by theoretical calculation. All parameters values used in the gain computation are enumerated in Table 1.

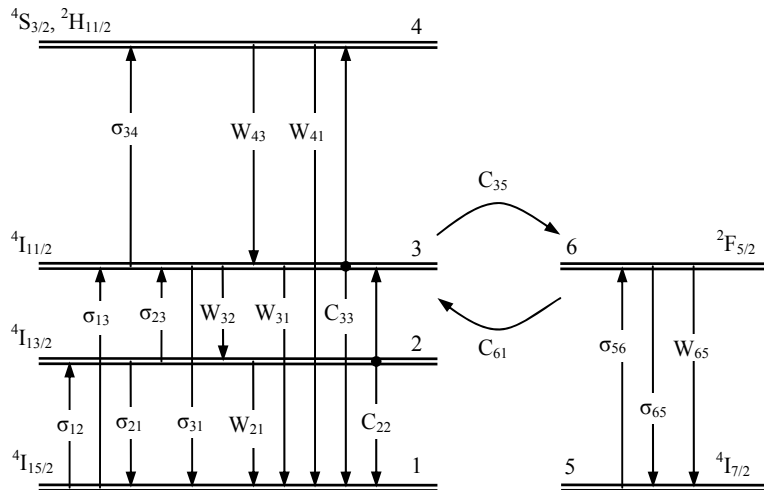


Fig 1. Energy level diagram of $\text{Er}^{3+}:\text{Yb}^{3+}$ codoped fiber laser

The rate equations:

$$\frac{\partial N_2}{\partial t} = \sigma_{12}\phi_s N_1 - \sigma_{21}\phi_s N_2 - \sigma_{23}\phi_s N_2 - W_{21}N_2 + W_{32}N_3 - 2C_{22}N_2^2 \quad (11)$$

$$\begin{aligned} \frac{\partial N_3}{\partial t} = & \sigma_{13}\phi_p N_1 - \sigma_{31}\phi_p N_3 + \sigma_{23}\phi_s N_2 - \sigma_{34}\phi_p N_3 - (W_{32} + W_{31})N_3 \\ & + W_{43}N_4 + C_{22}N_2^2 - 2C_{33}N_3^2 + C_{61}N_1N_6 - C_{35}N_3N_5 \end{aligned} \quad (12)$$

$$\frac{\partial N_4}{\partial t} = \sigma_{34}\phi_p N_3 - (W_{41} + W_{43})N_4 + C_{33}N_3^2 \quad (13)$$

$$N_{Er} = N_1 + N_2 + N_3 + N_4 \quad (14)$$

$$\frac{\partial N_6}{\partial t} = \sigma_{56}\phi_p N_5 - \sigma_{65}\phi_p N_6 - W_{65}N_6 + C_{35}N_3N_5 - C_{61}N_1N_6 \quad (15)$$

$$N_{Yb} = N_5 + N_6 \quad (16)$$

Table 1. Parameters value used in calculation

Symbol	Parameters	Value	Reference
λ_s	Signal wavelength	1530 nm	-
λ_p	Pump wavelength	980 nm	-
P_p	Pump power	150mW	-
L	DFB FL cavity length	50mm	-
σ_{12}	Absorption cross section of Er ³⁺ at λ_s	$8.9 \times 10^{-25} \text{ m}^2$	[14]
σ_{13}	Absorption cross section of Er ³⁺ at λ_p	$2 \times 10^{-25} \text{ m}^2$	[14]
σ_{21}	Emission cross section of Er ³⁺ at λ_s	$8.7 \times 10^{-25} \text{ m}^2$	[14]
σ_{31}	Emission cross section of Er ³⁺ at λ_p	$2 \times 10^{-25} \text{ m}^2$	[13]
σ_{56}	Absorption cross section of Yb ³⁺ at λ_p	$8.7 \times 10^{-25} \text{ m}^2$	[8]
σ_{65}	Emission cross section of Yb ³⁺ at λ_p	$11.6 \times 10^{-25} \text{ m}^2$	[8]
σ_{23}	ESA cross section of Er ³⁺ at λ_s	$1 \times 10^{-27} \text{ m}^2$	[15]
σ_{34}	ESA cross section of Er ³⁺ at λ_p	$1 \times 10^{-27} \text{ m}^2$	[15]
W_{21}	Spontaneous emission rate of Er ³⁺	100 s^{-1}	[15]
W_{32}	Nonradiative decay rate of Er ³⁺	100000 s^{-1}	[8]
W_{31}	Spontaneous emission rate of Er ³⁺	30000 s^{-1}	[8]
W_{41}	Spontaneous emission rate of Er ³⁺	100000 s^{-1}	[8]
W_{43}	Nonradiative decay rate of Er ³⁺	100 s^{-1}	[8]
W_{65}	Spontaneous emission rate of Yb ³⁺	1000 s^{-1}	[8]
C_{33}	Cooperative upconversion coefficient of Er ³⁺	$2.5 \times 10^{-21} \text{ m}^3 \text{ s}^{-1}$	[14]
C_{22}	Cooperative upconversion coefficient of Er ³⁺	$2.5 \times 10^{-21} \text{ m}^3 \text{ s}^{-1}$	[14]
C_{61}	Energy transfer coefficient Yb ³⁺ to Er ³⁺	$5 \times 10^{-21} \text{ m}^3 \text{ s}^{-1}$	[14]
C_{35}	Energy transfer coefficient Er ³⁺ to Yb ³⁺	$5 \times 10^{-21} \text{ m}^3 \text{ s}^{-1}$	[14]
α_s	Background loss at λ_s	0.15 m^{-1}	-
α_p	Background loss at λ_p	0.20 m^{-1}	-
N_{Er}	Total erbium ion population	$2.4 \times 10^{26} \text{ m}^{-3}$	-
N_{Yb}	Total ytterbium ion population	$1.2 \times 10^{25} \text{ m}^{-3}$	-
n_{eff}	Core effective refractive index	1.47	-
Δ	Index difference	9.3×10^{-3}	-
r	Core radius	2.3 μm	[16]
NA	Numerical aperture	0.20	[17]
Γ_p	Overlap factor at λ_p	0.64	[18]
Γ_s	Overlap factor at λ_s	0.43	-

Most fiber amplifiers are fabricated with small core size for higher pump intensity to achieve better inversion. The theoretical optimum value for core radius is between 2 and 3 μm [16], and in our case we select the radius of 2.3 μm . Numerical aperture for fiber amplifier is typically high compared to the standard single mode fiber for better small signal gain [17], and in our case we choose NA with value of 0.2. Fiber core refractive index, n_1 is assumed to have a value of 1.47, and the calculated cladding index, n_2 from $(n_1^2 - n_2^2)^{0.5} = \text{NA}$ formula is 1.456. The V numbers calculated using $V = 2\pi \text{NA}/\lambda$ for signal at 1530nm and pump at 980nm are 1.89 and 3.24 respectively. This indicates excitation of fundamental i.e. LP₀₁ for 1530nm signal, while LP₀₁ and LP₁₁ for 980nm pump. Since signal is single moded in the fiber, the spotsize can be determined using $\omega = r(0.65 + 1.619V^{-1.5} + 2.879V^{-6})$, yields value of 3.04 μm . Knowing the spotsize, overlap factor for signal with Gaussian beam approximation is calculated from $\Gamma_s = 1 - \exp(-r^2/\omega^2)$, thus the obtained value is $\Gamma_s = 0.43$. For pump that is not single moded in the fiber, the theoretical value of pump overlap factor, Γ_p for equally excited LP₀₁ and LP₁₁ is between 0.6 and 0.7 [18], and in this case we use the value of 0.64.

Numerical method such as Newton-Raphson can be utilized to solve the equations (11) to (16) simultaneously in steady state. By solving the rate equations, population at each energy level can be determined. Pump and signal growths over an infinitesimal length of DFB FL, dz are determined by simple one dimensional propagation equations as outlined by equations (17) and (18). From the pump propagation equation, it can be seen that the pump will be decayed over the cavity length due to the dominant losses mechanisms, i.e. the high absorption of Yb³⁺ to excite ions from level ⁴I_{7/2} to ²F_{5/2} as well as high absorption of Er³⁺ to excite ions from level ⁴I_{5/2} to ⁴I_{11/2}. From the signal propagation equation, the signal is apparently will be improved over the cavity by the high emission mechanism at the 1530nm wavelength, however the growth is not in exponential trend due feedback grating structure of the cavity. The propagation equations can be solved by using any numerical techniques such as the Euler and the Runge-Kutta methods.

$$\frac{dP_p}{dz} = (\sigma_{65}N_6 - \sigma_{56}N_5 + \sigma_{31}N_3 - \sigma_{13}N_1 - \sigma_{34}N_3)\Gamma_p P_p - \alpha_p \quad (17)$$

$$\frac{dP_s}{dz} = (\sigma_{21}N_2 - \sigma_{12}N_1 - \sigma_{23}N_2)\Gamma_s P_s - \alpha_s \quad (18)$$

2.3 Output power analysis method

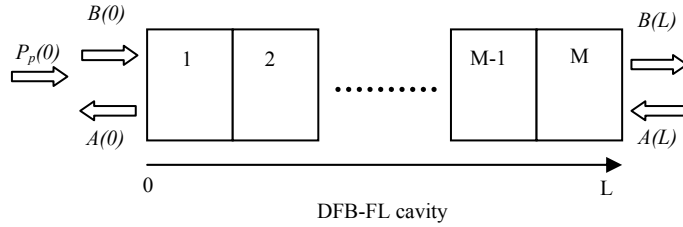


Fig 2. Schematic of DFB FL used in analysis

Figure 2 illustrates the convention used for modeling the output power with B denotes the forward propagating wave, A is the backward propagating wave, and block sections with numbers 1 to M are the corresponding cavity section. Number of sections, M used in our study is 100, which yields similar results as the larger number of section in range of 1000 to 10000. It should be noted that each of the cavity sections possess its own physical properties e.g. for the m^{th} section the corresponding parameters are A^m , γ^m , L^m and etc. The boundary condition to be fulfilled is zero input signal field at left and right ends of DFB FL i.e. $B(0) = A(L) = 0$. To begin the analysis, the forward propagating wave i.e. $B(0)$ is first set to 0, similar to the boundary condition. Trial values of λ_L and $A(0)$ values are initially used. The local signal power of the first section is then calculated by $|B|^2 + |A|^2$. With a pump power at $z=0$ and the previously calculated local signal power, the signal and pump power at the output of the first section can be determined by solving the rate equations, and hence signal gain and pump loss is known. The gain value is then used to calculate transfer matrix components of first section. Forward and backward signals at the input of the following section are then determined from the transfer matrix relation:

$$\begin{bmatrix} B_{m+1} \\ A_{m+1} \end{bmatrix} = \begin{bmatrix} T_{11}^m & T_{12}^m \\ T_{21}^m & T_{22}^m \end{bmatrix} \begin{bmatrix} B_m \\ A_m \end{bmatrix} \quad (19)$$

In case of phase shift, calculation of the forward and backward signals for the following section is given by:

$$\begin{bmatrix} B_{n+1} \\ A_{n+1} \end{bmatrix} = \begin{bmatrix} \exp(-\pi/2) & 0 \\ 0 & \exp(\pi/2) \end{bmatrix} \begin{bmatrix} B_n \\ A_n \end{bmatrix} \quad (20)$$

The calculation procedure is repeated until arrive at the DFB FL right end i.e. at $z=L$. At the DFB FL end, the boundary condition of $A(L)=0$ is tested, and in our calculation the value of $A(L)<10^{-5}$ is acceptable. If the condition is not fulfilled, the guessed values of λ_L and $A(0)$ are modified and the calculation procedure is then repeated. If the condition is fulfilled, λ_L is taken as the lasing wavelength, $|B(L)|^2$ as the output power at $z=L$, and $|A(0)|^2$ as output power at $z=0$.

2.4 Threshold gain analysis method

Analytical expression for the fundamental threshold gain of DFB FL with constant profile is given by [5]:

$$\gamma_{th} = 4\kappa_m \exp(-\kappa_m L) + \alpha_s \quad (21)$$

where α_s is the background loss or intrinsic unbleachable loss of the fiber laser. For apodized DFB FL with non-constant structure, the analytical approach is not applicable and therefore numerical method is employed. Threshold gain for DFB FL can be found by the above threshold condition defined by $T_{11}(1:M)=0$. $T_{11}(1:M)$ is the T_{11} value obtained from multiplication of the entire transfer matrix that is given by:

$$T(1|M) = \prod_1^M T^m \quad (22)$$

To fulfill the above threshold condition, the trial and error substitutions of λ_L and γ are required. The multiplication process of the entire transfer matrix is repeated until the above threshold condition is fulfilled and for this study $T_{11}(1:M)=10^{-6}$ is applied. The solution pair that is closest to the design wavelength, λ_B is the fundamental threshold. The solution found next to the fundamental threshold wavelength is the first higher order mode threshold and then followed by subsequent higher order mode threshold.

2.5 Apodization profiles

Three different profiles are considered in this study, the gaussian, sigmoid and flat profiles. The flat profile, that also known as the standard DBF FL, serves as a benchmark in our analysis. The gaussian [19] and sigmoid functions used in simulation are given by the following equations:

$$\kappa(z) = \kappa_m \exp\left[-0.5\left(\frac{z - z_{ps}}{a_1}\right)^2\right] \quad (23)$$

$$\kappa(z) = \kappa_m \left[1 + c \exp(-k |z - z_{ps}|)\right]^{-1} \quad (24)$$

where $\kappa(z)$ is spatial AC coupling coefficient, κ_m is peak coupling coefficient, z_{ps} is phase shift position in cavity, a_1 is defined as $a_1 = FWHM / \sqrt{8 \ln 2}$ and, c and k are minimum point and curve control variables respectively. The value of FWHM used for gaussian profile is $0.75L$ or 37.5mm , while c and k values used for sigmoid profile are 700 and 0.24 for number of point 100. The DFB FL cavity is symmetry to a centrally located phase shift. The profile shapes used in the analysis are illustrated in Figure 3.

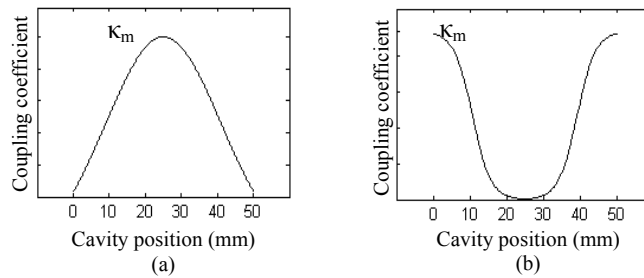


Fig 3. Profiles shape tested in model: (a) gaussian, and (b) sigmoid

3. RESULTS AND DISCUSSION

3.1 Output power

In the first analysis, the value of peak coupling coefficient is varied within all possible values for fundamental longitudinal mode lasing. Output power of the flat profile is used as a reference, where all results are normalized to the peak output power of the flat profile which is 7.07mW at $\kappa_m=185$ m. The plot of normalized output power against peak coupling coefficient, κ_m and effective grating strength, κL_{eff} are shown in Figure 4 and Figure 5 respectively. κL_{eff} is the mean value of $\kappa(z)$ that is obtained by integrating the profiles with respect to cavity length. The importance of plotting the results against κ_m and κL_{eff} values is that κ_m represents the actual value used in numerical model while κL_{eff} provides better comparison between profiles with different shapes. Since the output power is symmetrical for all profiles, i.e. $P_o(0)\approx P_o(L)$, only one plot is shown.

It is apparent from Figure 4 and Figure 5 that sigmoid profile demonstrates the highest peak output power, almost 1.5 times the peak value of the reference. High κ_m is required for sigmoid profile in lasing operation to compensate descending $\kappa(z)$ around central cavity of this profile. For example, at peak point, κ_m for sigmoid profile is 320, while for flat and gaussian are with lower values of 185 and 277 respectively as shown in Figure 4. The corresponding value κL_{eff} for sigmoid profile however is relatively low with value of 7.2 compared to 9.2 and 9.8 for flat and gaussian profile respectively. This result also suggests that certain apodization profile has the respectively optimum value of grating strength. The fundamental threshold of κL_{eff} can be determined from Figure 5 by observing the beginning of the lasing point. It is apparent sigmoid profile has the lowest κL_{eff} threshold around 3.8, compared to flat and sigmoid profiles with the value of 5.1. It is also noticeable that output power will be eventually reach zero when exceeding certain κL_{eff} , which indicates that, the fundamental longitudinal mode operation is no longer exist.

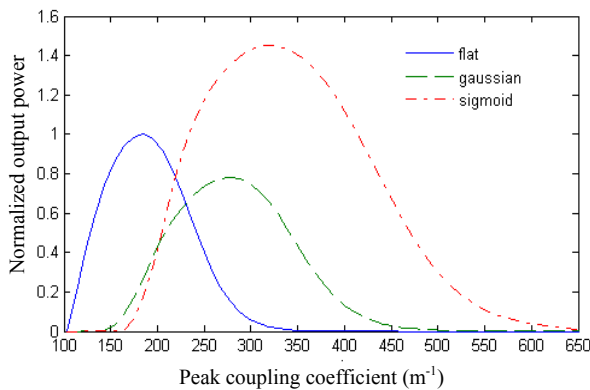


Fig 4. Normalized output power against peak coupling coefficient

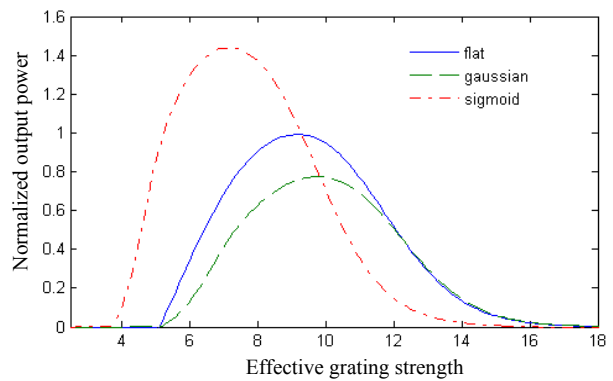


Fig 5. Normalized output power against effective grating strength

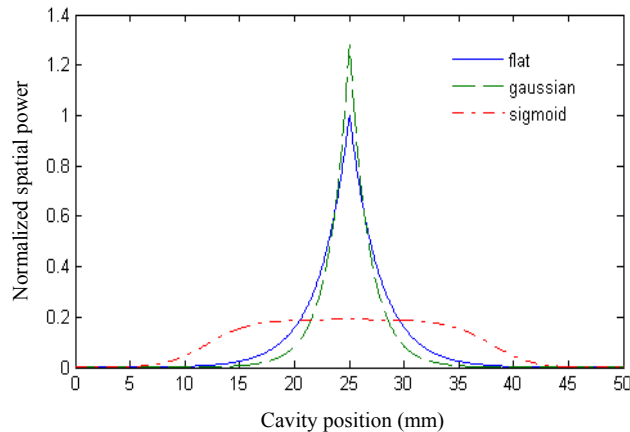


Fig 6. Normalized spatial power distribution

Figure 6 indicates spatial power distribution for peak output power of each profile, where all are normalized to peak distribution of flat profile DFB FL. This result explains the reason why sigmoid profile produces superior output power than other profiles. By applying the sigmoid profile i.e. by weakening the coupling coefficient around the phase shift, the spatial power is loosely confined in cavity. Sigmoid profile enables the spatial power to develop faster from left and right ends of cavity due to high $\kappa(z)$ region here, and continue to remain low around z_{ps} as it is a low $\kappa(z)$ region. This allows a more effective use of cavity length compared to other profiles. In contrast, gaussian profile has more tightly confined spatial power and spatial power is concentrated around the phase shift, thus reducing the effective cavity length

3.2 Fundamental and higher order mode threshold

The operation of DFB FL at multiple wavelengths is undesired in some applications. In the presence of external perturbation, DFB FL that operates near the threshold is exposed to the risk of mode hopping which consequence adverse effects highly sensitive system. For laser that operates in stable dual longitudinal operation could be useful for microwave signal generation while the laser with unstable operation is normally have to be avoided. Figure 7 shows typical operations of multi longitudinal mode operation of DFB FL. As the gain induced by pump exceeds the threshold gain, DFB FL lases at multiple wavelength which drifted away from the design wavelength. The lasing wavelengths are further detuned from the design wavelength as the gain induced by pump is increased.

The numerical model used is verified by comparing the calculated result using the TMM with the one obtained from the analytical model given by $\gamma_{th} = 4\kappa_m \exp(-\kappa_m L) + \alpha_s$ for flat profile DFB FL. Figure 8 shows the resulting plot, which indicate similar to the numerical result to the analytical result. Hence, we verify that our numerical model produces satisfactory accuracy to be further implemented in analyzing different DFB FL profiles.

Figure 9 shows fundamental mode threshold gain, γ_{th} against effective grating strength, κL_{eff} for all profiles. For κL_{eff} smaller than 8, it is obvious that gaussian profile has the highest fundamental γ_{th} compared to other profiles. In contrast, sigmoid profile has the lowest fundamental γ_{th} , which manifests the lowest threshold pump at certain κL_{eff} . It is also apparent that the fundamental γ_{th} for κL_{eff} above 8 is dominated by the α_s , and in this study the value is 0.15 m^{-1} or 0.65 dBm^{-1} . Hence, minimization of α_s is necessary to not only reduce the fundamental threshold gain, but also to improve the output power at certain pump level.

The γ_{th} of the first and second higher order mode i.e. +1/-1 and +2/-2 mode for gaussian and flat profile are shown in Figure 10. Sigmoid profile is omitted since it has much lower threshold value than the other two profiles. As illustrated in Figure 10, the higher order γ_{th} of flat profile decreases steadily as κL_{eff} increases. At the highest κL_{eff} value indicated in Figure 10 which is 14, the corresponding +1/-1 γ_{th} is 7.2 dBm^{-1} . It is strongly believed that the +1/-1 γ_{th} will be further decrease below 7.2 dBm^{-1} as κL_{eff} exceeds 14. This suggests that DFB FL could possibly reach the first higher order mode threshold with sufficiently high κL_{eff} for flat profile. For the gaussian profile, the higher order γ_{th} trend is somehow different from the flat profile. The +1/-1 γ_{th} has an increasing trend toward high κL_{eff} after a temporary dip at κL_{eff} equal to 7.5. At higher κL_{eff} , between 11 and 14, it is observed that the +1/-1 and +2/-2 γ_{th} are very close to each other and this phenomena is more evident for gaussian profile than on flat profile. This signifies that +1/-1 and +2/-2 modes could be combined into a single longitudinal mode, with formation of other modes at other wavelength. Figure 11 shows the margin between fundamental and first higher order mode threshold gain. Obviously, the gaussian profile possesses better threshold margin compared to the flat profile.

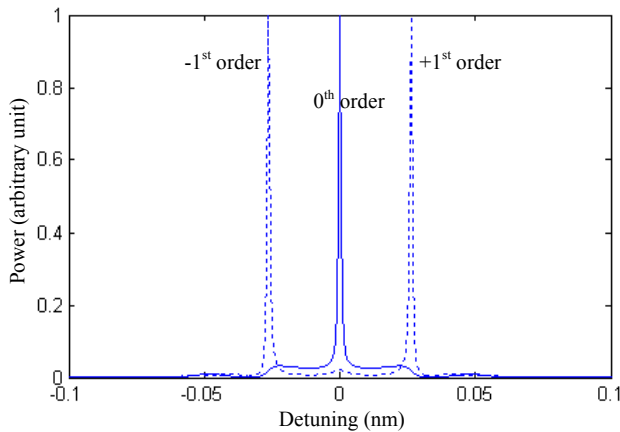


Fig 7. Normalized first higher order mode spectrum detuned from the designed wavelength

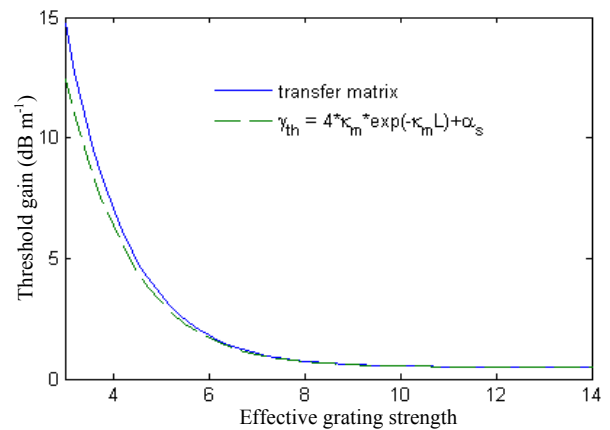


Fig 8. Fundamental mode threshold gain obtained from the TMM and analytical model, calculated for the flat profile

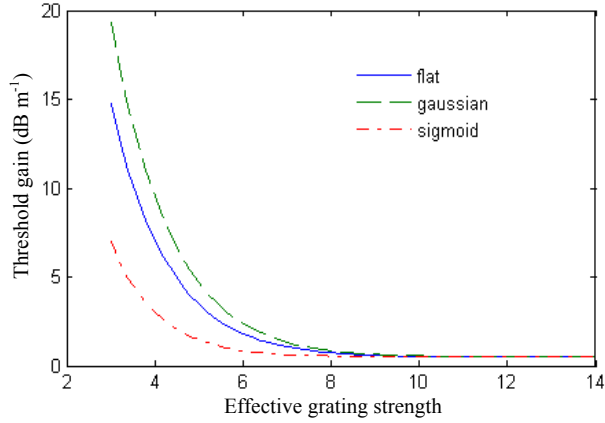


Fig 9. Fundamental mode threshold

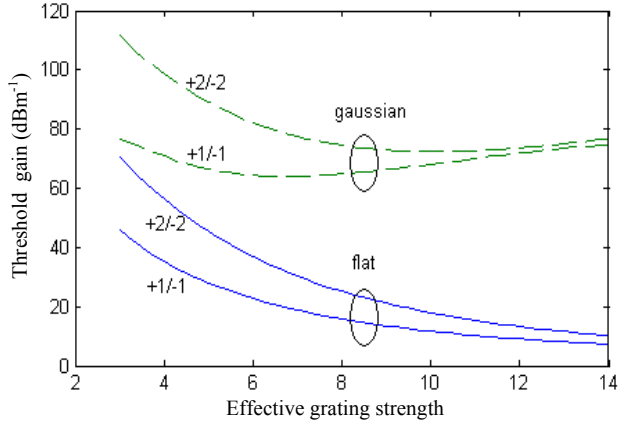


Fig 10. Higher order mode threshold

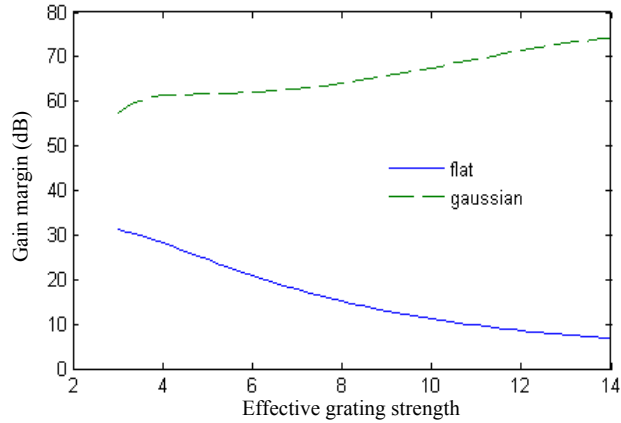


Fig 11. Threshold margin between fundamental and first higher order mode

3.3 Performance tradeoffs

Apparently, the three different profiles used in the simulation are differentiated by the shape around z_{ps} which exhibit different characteristics. Suppression of sidelobes by mean of gaussian apodization, which is also applied in FBG design, will enhance threshold margin between fundamental and first higher order mode. This type of profile could also be employed in densely arrayed system to minimize the excess phase noise by reducing the cross coupling effect originated from out of band reflection of sidelobes [20]. Another possible advantage is that, this profile allows the utilization of high κL_{eff} gratings in DFB FL design while maintaining high threshold margin. Since linewidth of DFB FL is proportional to $1/\kappa^2 L^3$ [21], it is desirable to fabricate DFB FL with high κL_{eff} to yield a very low linewidth suitable for sensing application. In conjunction with high κL_{eff} design, utilization of highly concentrated fiber such as phosphate based fiber for higher net gain while maintaining single longitudinal mode operation is possible. Previously, it has been demonstrated that a flat profile DFB FL with $\kappa L_{eff} > 14$ exhibits dual wavelength operation [22], and it is strongly believed that such problem can be overcome by apodization. Although this profile demonstrated to have the lowest output power, it does not pose any significant disadvantages for practical utilizations. On the other hand, by applying a profile that is weak around the phase shift will have advantage of superior output power due to the effective use of cavity length for conversion. However, this type of profile has a major disadvantage of low threshold margin that causes instability to single longitudinal mode operation. One should also realize that sigmoid apodization is nearly resemblance to Fabry-Perot configuration i.e. the distributed Bragg reflector fiber laser (DBR FL), hence its characteristics is close to DBR FL. Finally, the flat profile possesses an intermediate performance between the other two profiles. Due to the straightforward design, the flat profile has an advantage of fabrication simplicity, thus minimizing risk of error in fabrication.

4. CONCLUSIONS

The output power and threshold characteristics of apodized DFB FL are investigated in this paper. In the output power analysis, it is demonstrated that certain profile has the optimum value of κL_{eff} . Apodization technique can enhance the output power of DFB FL as demonstrated by the sigmoid profile. Result gained from the output power analysis can be used to determine the fundamental threshold gain parameter of apodized DFB FL for a certain pump power. Another important purposes of apodization technique is to improve the threshold margin between the fundamental and the first higher order mode of DFB FL as demonstrated by the gaussian profile. The types of apodization function used are not limited to those used in this paper, where different functions are possible to be utilized to achieve better performance. By implementing apodization technique, there will be some tradeoffs in DFB FL design. Therefore, optimization of certain parameters can be made to suit the need of particular applications. The improvements achieved will benefit system level performance for variety of applications.

REFERENCES

- [1] Voo, N. Y., Horak, P., Ibsen, M. and Loh, W. H., "Anomalous linewidth behavior in short cavity single frequency fiber laser," IEEE Photonics Technology Letters 17(3), 546-548 (2005).
- [2] Hill, D.J., et al., "DFB fibre-laser sensor developments," Proc. SPIE, 5855 Part II, 904-907 (2005).
- [3] Foster, S., et al., "A fibre laser hydrophone," Proc. SPIE, 5855 Part II, 627-630 (2005).
- [4] Cranch, G. A., Nash, P. J. and Kirkendall C. K., "Large-scale remotely interrogated arrays of fiber-optic interferometric sensors for underwater acoustic applications," IEEE Sensors Journal 3(1), 19-30 (2003).
- [5] Lovseth, S. W. and Ronnekleiv, E., "Fundamental and higher order mode thresholds of DFB fiber lasers," Journal of Lightwave Technology 20(3), 494-501 (2003).
- [6] Aseev, V. A., et al., "How the ytterbium concentration affects the population inversion of erbium in phosphate laser glasses," Journal of Optical Technology (A Translation of Opticheskii Zhurnal) 74(11), 769-772 (2007).
- [7] Lee, Y. W., et al., "20 W single-mode Yb³⁺-doped phosphate fiber laser," Opt. Lett 31(22), 3255-3257 (2006).
- [8] Jiang, C., Hu, W. and Zeng, Q., "Improved gain performance of high concentration Er³⁺-Yb³⁺ codoped phosphate fiber amplifier," IEEE Journal of Quantum Electronics 41(5), 704-708 (2005)
- [9] Lauridsen, V.C., Povlsen, J. H. and Varming, P., "Design of DFB fibre lasers," Electronics Letters 34(21) 2028-2030 (1998).
- [10] Lo, S. K. B. and Ghafouri-Shiraz, H., "Method to determine the above-threshold stability of distributed feedback semiconductor laser diodes," Journal of Lightwave Technology 13(4), 563-568 (1995).
- [11] Yariv, A., [Optical Electronics in Modern Communications 5th ed], Oxford University Press Inc., New York, 233 (1997).
- [12] Karasek, M., "Optimum design of Er³⁺-Yb³⁺ codoped fibers for large-signal high-pump-power applications," IEEE Journal of Quantum Electronics 33(10), 1699-1705 (1997).
- [13] Strohhofer, C. and Polman, A., "Relationship between gain and Yb³⁺ concentration in Er³⁺-Yb³⁺ doped waveguide amplifiers," Journal of Applied Physics 90(9): 4314-20 (2001).
- [14] Hadel, O., [Distributed feedback fibre laser strain and temperature sensors], Ph.D. dissertation, University of Southampton, Southampton. 33-37 (2001).
- [15] Yelen, K., Hickey, L. M. B. and Zervas, M. N., "Experimentally verified modeling of erbium-ytterbium co-doped DFB fiber lasers," Journal of Lightwave Technology, 23(3), 1380-1392 (2005).
- [16] Becker, P. C., Olsson, N. A. and Simpson, J.R., [Erbium-Doped Fiber Amplifiers: Fundamentals and Technology], Academic Press, San Diego, 180-181 (1999).
- [17] Dignonnet, M. J. F., "Closed-form expressions for the gain in three- and four-level laser fibers," IEEE Journal of Quantum Electronics 26(10), 1788-1796 (1990).
- [18] Desurvire, E., Zyskind, J. L. and Giles, C. R.. "Design optimization for efficient erbium-doped fiber amplifiers," Journal of Lightwave Technology 8(11), 1730-1741 (1990).
- [19] Othonos, A. and Kalli, K., [Fiber Bragg Gratings: Fundamentals and Applications in Telecommunications and Sensing], Artech House, Norwood, 198-199 (1999).
- [20] Tikhomirov, A. and Foster, S., "DFB FL sensor cross-coupling reduction," Journal of Lightwave Technology 25(2), 533-538 (2007).

- [21] Kojima, K., Kyuma, K. and Nakayama, T., "Analysis of the spectral linewidth of distributed feedback laser diodes," *Journal of Lightwave Technology* 3(5), 1048-1055 (1985).
- [22] Ronnekleiv, E., Ibsen, M., Zervas, M. N. and Laming, R. I., "Characterization of fiber distributed-feedback lasers with an index perturbation method," *Applied Optics* 38(21), 4558-4565 (1999).